Current Science
CS 6 (1), 5952-5970 (2026)
Received 14 January 2026 | **Accepted 23 February** 2026 | **Online Available 28 February** 2026
https://doi.org/10.52845/CS/2026-6-1-23

Current Science

Current Science

OPEN ACCESS

ISSN (O) 2795-8639

Original Article

A Precision Monitoring Method for Corn Leaf Mite Damage Based on UAV Multispectral Data

Jingwei Bao[12], Pengbin Dong[1], Xinyao Kou[1], Jiahao Lai[1], Shuxing Tian[1] and Dongsheng Kong[13*]

[1]College of Agriculture and Ecological Engineering, HeXi University, Zhangye, 734000, China

[2]Ministry of Agriculture and Rural Affairs Research Base for Full-Process Mechanization of Corn Seed Production, HeXi University, Zhangye, 734000, China

[3]Research Institute for Rural Revitalization, HeXi University, Zhangye, 734000, China

***Corresponding Author: Dongsheng Kong**

Abstract:
The corn leaf mite (CLM) is one of the most destructive pests in corn seed production, seriously affecting the yield and quality of corn seeds. UAV-based remote sensing data offers a promising approach for efficiently monitoring CLM under field conditions. However, its performance may be affected by the mechanisms by which CLM piercing-sucking pests cause damage and by field conditions. In contrast, UAV-based fusion of spectral and textural data can improve monitoring accuracy by capturing complementary information from the internal and external aspects of corn leaves. However, there is still a lack of a method for optimizing texture features to achieve precise and efficient monitoring of CLM. This study introduces an index-combination method based on texture indices (TIs) to extract key spatial information from UAV multispectral data for early monitoring of CLM. Initially, a total of 18 vegetation indices (VIs) were extracted from multispectral images captured by UAVs, along with the simultaneous construction of three texture indices derived from textural characteristics. Following this, the Otsu-CIgreen algorithm was employed to determine the best threshold for removing the complex background of the image. Finally, based on the screened VIs and the fused features of VIs and TIs, three machine learning models were used to construct a CLM monitoring model. Among these models, the back propagation neural network (BPNN) model that integrates VIs and TIs performed best, achieving an accuracy of 93.47% and an F1 score of 93.64% on the test set. The results indicate: (1) The BPNN model based on the fusion of VIs and TIs is most effective for CLM monitoring, compared with VIs alone, the fusion of VIs and TIs significantly improves the accuracy of CLM monitoring; (2) Considering the different importance of texture features (TFs) and TIs, the VIs were fused separately with TFs and TIs. The BPNN model based on exponential fusion achieved the highest monitoring accuracy (accuracy: 93.47%, F1: 93.64%); compared with feature fusion, the test set showed improvements (accuracy: 90.00%, F1: 89.67%). The inclusion of texture indices significantly improved the sensitivity and accuracy of early CLM stress detection, providing an effective remote sensing technical pathway for early monitoring and precise prevention and control of CLM, which aids decision-making in smart agriculture and reduces pesticide use.

Keywords: Machine Learning; Corn Leaf Mite; Multispectral Images; Textural Indices

1. Introduction

Seeds are the "chip" of the corn industry, and their yield and quality directly affect production safety and industry benefits [1]. However, corn seed production faces a serious threat from devastating pests, such as the corn leaf mites (CLM) [2,3]. CLM outbreaks rapidly under high-temperature,

low-humidity conditions, feeding by piercing–sucking on the undersides of maize leaves and consuming the sap, causing leaves to lose their green color and turn yellow, and exhibiting sudden and devastating damage characteristics. CLM mainly occurs during the middle to late stages of corn development, especially from tasseling to the grain-filling stage. widespread in warm regions of the world and causing serious yield losses. In recent years, studies have indicated a significant increase in the incidence of CLM, particularly in western China. This trend may be attributed to climate change, continuous cropping practices, and the lack of insect-resistant varieties [4,5]. Therefore, obtaining accurate spatial information on whether early CLM has occurred under field conditions is crucial for precision field management practices in corn seed production (such as pesticide application).

Traditional methods of obtaining pest information include onsite visits and manual surveys, which tend to be labor-intensive, subjective, and time-consuming [6]. On the other hand, remote sensing offers a more efficient solution for tracking crop pests, allowing extensive coverage over various spatial and temporal dimensions [7]. Recently, advances in unmanned aerial vehicle (UAV) remote sensing technologies have introduced enhanced techniques for monitoring crop pests, thanks to their flexible data collection capabilities and excellent spatiotemporal resolution [8].

The measurement of spectral reflectance provides insights into both biophysical and biochemical parameters, thereby effectively indicating the health status of crops [6]. Low-altitude imaging performed by drones is frequently employed for monitoring pests in crops [9,10], including species such as goji gall mites and corn aphids. Nevertheless, there are limitations associated with drone-based multispectral imaging, as these techniques can exclusively gather spectral data from leaves, which reduces their capability to effectively monitor crop pests in field environments [11]. Moreover, relevant research suggests that corn plants are especially vulnerable to CLM infections when subjected to drought and elevated temperatures, which aids the transmission of CLM to adjacent plants. In addition, the use of texture information is expected to improve CLM measurements under field conditions, because it can capture the spatial distribution of pixel values within local regions of an image, effectively complementing the limitations of spectral information [12]. Recent studies have emphasized the potential of texture information to complement spectral information in plant pest and disease monitoring, for example in monitoring peanut southern blight and corn army worm [13,14]. However, research on using drones to monitor CLM based on spectral and texture information remains limited. UAV-based spectral and texture data can capture different complementary information about the internal and spatial characteristics of crop pests. Although texture features and their indexing have been widely applied in crop pest and disease monitoring (e.g., in tomatoes or forest pests), their potential for early diagnosis of maize leaf mite damage—especially through the integration of optimized texture indices with spectral indices—still warrants further exploration. Therefore, it remains necessary to exploit complementary spectral and textural information to improve the early monitoring accuracy of CLM. Traditional machine learning algorithms, including Particle Swarm Optimization Support Vector Machine (PSO-SVM) [14], Back Propagation Neural Network (BPNN) [15], and Extreme Gradient Boosting (XGBoost) [16], have been proven effective in crop pest monitoring. These studies employed optimal feature selection methods to mitigate data redundancy and retain the key information for crop pest monitoring (specific spectral features) [17,18]. However, these methods ignore the unequal importance of different inputs in feature fusion, thereby potentially limiting the effectiveness of fusing spectral and texture information for CLM monitoring. Today, machine learning algorithms have demonstrated tremendous potential in crop pest monitoring. Previously, most machine learning research in this field primarily focused on algorithm development [19,20], with models concentrating on extracting spectral information while overlooking the significant advantages of spatial information in pest detection. However, TFs can effectively supplement information about plant surface morphology and spatial distribution, enabling the model to better distinguish between healthy and affected plants and to maintain strong discriminative power even in field environments with complex backgrounds or varying illumination [21,22]. This could therefore improve the accuracy of early CLM monitoring

[23].

Currently, most studies use texture features and their indices to monitor plant pests and diseases, but their effectiveness for early CLM damage monitoring has not been confirmed. This study investigates the effectiveness of combining spectral and textural information for early monitoring of CLM damage, thereby uncovering the potential for monitoring CLM hazards. First, the Otsu-CIgreen algorithm combined with multispectral images will be used to determine the optimal threshold for background removal. Next, three TIs will be constructed based on different TFs to assess whether these indices can be applied more effectively to CLM monitoring. Finally, based on the selected optimal model, the accuracy of CLM monitoring using data combining VIs with TFs and using data combining VIs with TIs will be compared, and that model will be used to evaluate the stability and accuracy of fusing VIs and TIs for CLM monitoring.

2. Materials and Methods

2.1. Study Area

The experimental area is located at the Maojiawan corn seed production base (Fig. 1) in Ganzhou District, Zhangye City, Gansu Province, China. The area is situated at 38°83′02″ N, 100°22′54″ E, with an average annual sunshine duration of about 3000 h and an elevation of approximately 1497 m. The region features a typical temperate continental arid climate, characterized by intense solar radiation and significant diurnal temperature variations. With an average annual precipitation of 129mm and relative humidity around 51%, it provides an ideal environment for natural CLM infection, making it recognized as a natural hybrid corn seed production center. This study used the "DF899" corn variety planted on April 26, 2024. The experimental plots selected for this experiment received the same management measures for irrigation, fertilization, and so on. Field surveys indicate that CLM was the only stressor in the corn field, and no pesticides were applied. CLM was observed to occur naturally at the trial site at the end of July 2024.

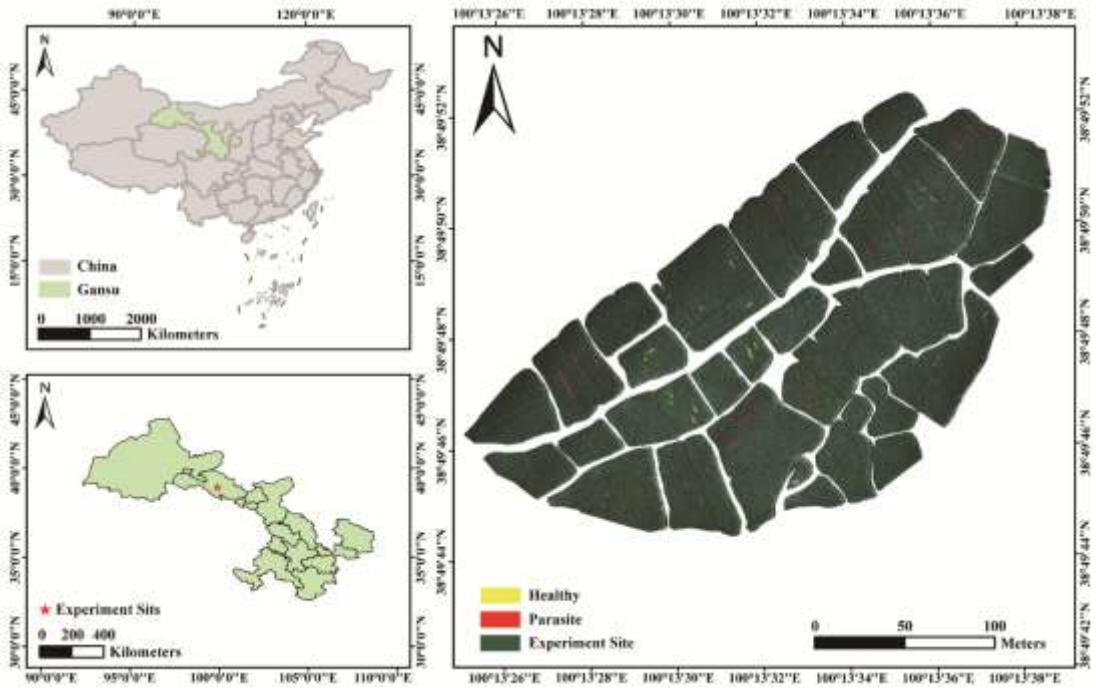

Figure 1. Study area and distribution of CLM samples.

2.2. UAV Data Acquisition and Preprocessing

In this research, the acquisition platform utilized was a DJI Mavic 3 Multispectral quadcopter UAV provided by Shenzhen DJI Innovation Technology Co. Ltd. This UAV has a weight of 0.951 kg and features five sensors: one color sensor for visible imaging and four monochrome sensors designated

for multispectral imaging, which are Green (G), Red (R), Rededge (RE), and Near-infrared (NIR). Each sensor's effective pixel count is 5.00 million, with the specifications for each sensor band outlined in Table 1. The UAV captured multispectral images during the period between 11:00 and 14:00 on August 7, 2024, under sunny conditions with no wind and excellent visibility. The UAV operated at a flight altitude of 50 m and a speed of 4.4 m/s, taking photos at 2-second intervals. The heading overlap during flight was recorded at 70%, while the side overlap reached 80%, resulting in an image resolution of 1.0 cm/pixel. The reflectance values of the calibration panels employed in this experiment were measured at 0.25 and 0.5, respectively. Following the importation of images into the DJI Terra software for radiometric correction and stitching, four single-channel reflectance images were produced. Subsequently, ENVI 5.3 software was used to combine these single-channel reflectance images into a composite 4-channel multispectral image.

Table.1 Multispectral sensor parameters

Band	Center wavelength (nm)	Band-width (nm)
Green	560 nm	16 nm
Red	650 nm	16 nm
Rededge	730 nm	16 nm
Near-infrared	860 nm	26 nm

2.3. Ground Data Collection

According to the local standards "Technical Specifications for Corn Leaf Mite Monitoring and Reporting" (DB 64/T 1797—2021) and "Survey Specifications for Monitoring the Corn Red Index" (DB 14/T 907-2014), experts use four corn plants as one sampling point, take the average, and visually assess the occurrence of CLM. Sample points were classified by occurrence level: levels 0 and 1 were designated as healthy sample points, and levels 2, 3, and 4 as pest-infested sample points（Table.2）. At the beginning of August 2024, during the corn tasseling stage, visual inspections were carried out in the experimental field; 60 healthy sample points and 80 pest-damaged sample points were randomly selected and split into training and test sets in a 7:3 ratio. Using the DJI Mavic 3 multispectral quadcopter drone's Real-Time Kinematic (RTK) capability, the WGS-84 coordinate information at the center of each sampling point is recorded, with horizontal positioning accuracy of approximately 0.02 m.

Table.2 Classification criteria for corn leaf mite damage

Healthy	Level 0	Harmless
	Level 1	No netting on the leaves, or only a small amount of netting on the lower leaves, with the netted area accounting for less than 5% of the leaf area.
Parasite	Level 2	The netted portion of the leaf's main vein is less than one-third of the main vein's length, and the two leaves below the ear have no netting.
	Level 3	The netting on the midrib of the two leaves below the spike is less than two-thirds of the midrib's length, and the two leaves above the spike have sporadic netting.
	Level 4	The leaves above and below the ear show pronounced netting; the netting along the midrib extends for more than two-thirds of the midrib length, and the leaves lose their green color and turn yellow.

2.4. Feature Selection and Classification Algorithms

The RF algorithm was employed in this research for the purpose of selecting features. Feature selection was conducted using the RF algorithm in this study

[24,25]. The RF method is composed of numerous decision trees, which collectively analyze various perspectives to assess the significance of features, instead of depending on just one decision tree [24]. Otsu's algorithm is an adaptive thresholding segmentation method based on the criterion of maximizing between-class variance, it divides image pixels into foreground and background classes using histogram statistics. The method searches through all possible gray-level thresholds and selects the threshold that maximizes the difference between the two classes as the optimal segmentation point, and it does not require manual parameter setting [26].

Back Propagation Neural Network (BPNN)

BPNN is a multilayer feedforward neural network that iteratively updates weights via error backpropagation, has strong nonlinear fitting capability, is suitable for complex input–output mappings [27], and has shown outstanding performance in pest and disease identification, remote sensing classification, and environmental monitoring [13,28,29]. BPNN, through a multi-layer neuronal structure and nonlinear activation functions, can learn and extract deep, abstract features from spectral and texture data, thereby better capturing the complex, nonlinear physiological, biochemical, and morphological changes in plants caused by corn leaf mite damage. In this experiment, a grid search method was used to find the optimal model parameters.

Particle Swarm Optimization Support Vector Machine (PSO-SVM)

PSO-SVM constructs nonlinear classifiers using kernel methods, with computational complexity depending on the support vectors rather than the dimensionality. When combined with particle swarm optimization, it can efficiently optimize parameters, thereby improving the SVM's generalization performance and stability, making it suitable for high-dimensional, small-sample, and strongly nonlinear tasks [30]. PSO-SVM achieves binary classification by constructing an optimal separating hyperplane that maximizes the margin between the two classes of samples, thereby effectively separating healthy and pest-infested samples in the feature space. PSO-SVM combines SVM’s advantages in handling high-dimensional, small-sample data with PSO’s global optimization capability, and has been widely applied in agricultural pest monitoring and growth assessment [31,32]. In this experiment, the PSO algorithm was used to optimize the gamma and c parameters.

Extreme Gradient Boosting (XGBoost)

XGBoost is an efficient and scalable ensemble learning algorithm that uses gradient boosting to combine weak trees, progressively minimizing loss; it offers feature selection and generalization capabilities and can effectively suppress overfitting. XGBoost performs a second-order Taylor expansion of the loss function and incorporates optimization strategies such as parallel computation and sparsity awareness, enabling it to exhibit excellent robustness, generalization, and efficiency when handling nonlinear relationships, feature interactions, and multispectral data with missing values, and to output feature importances that explain each index's contribution. It is widely applied to pest and disease monitoring, yield prediction, and multi-source remote sensing fu-sion [9,12,33]. In this experiment, grid search was used to find the best model parameters.

2.5. Extraction of VIs

To monitor CLM effectively, this research chose 18 VIs that are especially sensitive to the conditions affecting plant growth. VIs are derived from linear or nonlinear combinations of various remote sensing spectral bands, reflecting vegetation’s vigor and activity [34]. When subjected to stress, crops experience notable changes in both their physiological and morphological indicators [35,36]. Utilizing different VIs allows for the effective capture and digital representation of these changes.

Because CLM damage causes leaves to lose their green color and turn yellow, this study selected several indicators that can reflect chlorophyll content and insect pest stress, such as relative growth rate (RGR), green difference vegetation index (GDVI), and rededge chlorophyll index (CIrededge). In addition, it also includes several commonly used VIs, such as the Normalized Difference Vegetation Index (NDVI), the Leaf Chlorophyll Index (LCI), and the Optimized Soil-Adjusted Vegetation Index (OSAVI). By integrating these indicators, the growth status of corn and the extent of leaf mite damage can be evaluated more comprehensively, providing a quantitative basis for early pest monitoring and precise control. The calculation formulas of VIs used in this article are shown in Table 3.

Table 3 Formula for Calculating Vegetation Index

Name of index	Calculation formula	References
Normalized Difference Vegetation Index (NDVI)	$NDVI=(nir-r)/(nir+r)$	[37]
Optimized Soil Adjusted Vegetation Index (OSAVI)	$OSAVI=(nir-r)/(nir+r+0.16)$	[38]
Rededge-Red Ratio Index 2 (RRI2)	$RRI2=re/r$	[39]
Red-Green Ratio (RGR)	$RGR=r/g$	[40]
Renormalized Difference Vegetation Index (RDVI)	$RDVI=nir-r/\sqrt{nir+r}$	[40]
Normalized Red-RE (NormRRE)	$NormRRE=re/(nir+re+g)$	[41]
Normalized Difference Vegetation Index rededge (NDVIrededge)	$NDVIrededge=(re-r)/(re+r)$	[42]
Normalized Difference Rededge (NDRE)	$NDRE=(nir-re)/(nir+re)$	[43]
Modified Simple Ratio (MSR)	$MSR=r/\sqrt{\frac{nir}{r}+1}$	[40] [44] [41]
Green Difference Vegetation Index (GDVI)	$GDVI=nir-g$	[45]
Difference Vegetation Index-Rededge (DVIRE)	$DVIRE=nir-re$	[45]
Chlorophyll Index rededge (CIrededge)	$CIrededge=nir/re-1$	[44]
Chlorophyll Index green (CIgreen)	$CIgreen=nir/g-1$	[46]
Canopy Chlorophyll Contents Index (CCCI)	$CCCI=\frac{(nir-re)/(nir+re)}{(nir-r)/(nir+r)}$	[47] [48]
Green Normalized Difference Vegetation Index (GNDVI)	$GNDVI=(nir-g)/(nir+g)$	[49]
Leaf Chlorophyll Index (LCI)	$LCI=(nir-re)/(nir+re)$	
Green-Red Vegetation Index (GRVI)	$GRVI=nir/g$	
Difference Vegetation Index (DVI)	$DVI=nir-r$	

2.6. Construction of TIs

Research indicates that TFs greatly enhance the precision of identifying and detecting pests and diseases in crops, which mirrors the physical traits and growth conditions of crop leaves [50-54]. When crops are attacked by pests, the color, morphology, and structure of leaf surfaces change, causing alterations in texture [55]. TFs can be extracted using the Gray-Level Co-occurrence Matrix (GLCM). This matrix accurately predicts and reflects comprehensive information such as the direction, adjacent intervals, and variation amplitude of grayscale values [56]. This study extracted four TFs sensitive to plant pest and disease monitoring: mean value, homogeneity, entropy, and correlation [13]. These features respectively reflect the overall brightness level of leaf images, the similarity of local pixels, information uncertainty, and the linear dependency between gray values. Table 4 lists the calculation formulas for the four TFs.

Table 4 Formulas for calculating the four texture features used in this study

Name of index	Calculation formula
Mean (Mea)	$Mea=\sum_{x,y=1}^{g} xP(x,y)$
Homogeneity (Hom)	$Hom=\sum_{x=1}^{G}\sum_{y=1}^{G}\frac{p(x,y)}{1+(x-y)^2}$
Entropy (Ent)	$Ent=\sum_{x=1}^{G}\sum_{y=1}^{G}p(x,y)\log p(x,y)$
Correlation (Cor)	$Cor=\sum_{x=1}^{G}\sum_{y=1}^{G}\frac{(x-Mean)(y-Mean)P(x,y)}{VAR}$

X and y represent the row and column indices of the image, respectively; P(x,y) represents the relative frequency of two neighboring pixels;$VAR = \sum_{x=1}^{G}\sum_{y=1}^{G}(x - Mean)^2\, P(x,y)$

TFs demonstrate high sensitivity and robustness in pest and disease monitoring and can significantly improve the diagnostic performance of models [9,56-61]. Although TFs offer significant advantages in pest and disease monitoring, their performance has been suboptimal in some previous studies [60,62,63]. However, constructing novel TIs can significantly improve the estimation accuracy of pest-related physiological parameters [52]. Based on previous research [13], this study selected and applied three composite (normalized difference, difference, ratio) TIs: NDTI, DTI, and RTI, with the aim of fusing the complementary information of four TFs and fully exploring their potential for crop pest monitoring.

$$NDTI=\frac{(T1-T2)}{(T1+T2)} \quad (1)$$

$$DTI=T1-T2 \quad (2)$$

$$RTI=T1/T2 \quad (3)$$

where T1 and T2 represent two different GLCM-based TFs

2.7. Model evaluation indicators

The monitoring performance of six models was assessed using accuracy, precision, recall, and the F1 score. The formula for calculating accuracy is outlined as follows:

$$Accuracy=\frac{TP+TN}{TP+TN+FP+FN} \quad (4)$$

$$Precision=\frac{TP}{TP+FP} \quad (5)$$

$$Recall=\frac{TP}{TP+FN} \quad (6)$$

$$F1score=\frac{2*(Precision*Recall)}{(Precision+Recall)} \quad (7)$$

True positive is denoted by TP, while false positive is indicated by FP. True negative is represented as TN, and false negative corresponds to FN

3. Results

3.1. Background Removal Based on Otsu-Cigreen

Disturbances like soil interference and shading can jeopardize the precision of pest monitoring. Consequently, this research seeks to investigate the effectiveness of employing various VIs alongside four raw spectral bands to address intricate backgrounds. Initially, ground survey data points will be utilized to conduct a statistical analysis of the imagery, examining the spectral variations between soil and corn plants. Fig. 2 illustrates the reflectance for 18 VIs and the four original spectral bands. As shown in the figure, the spectral reflectance of soil and corn exhibits the most pronounced differences in the CIgreen. Therefore,

the Otsu-Clgreen algorithm is used to obtain the optimal threshold and generate a binary mask image to remove the background of the multispectral image. Otsu-Clgreen is capable of effectively highlighting variations in the chlorophyll content of vegetation, thus enhancing the reflectance differences observed between soil and corn plants.

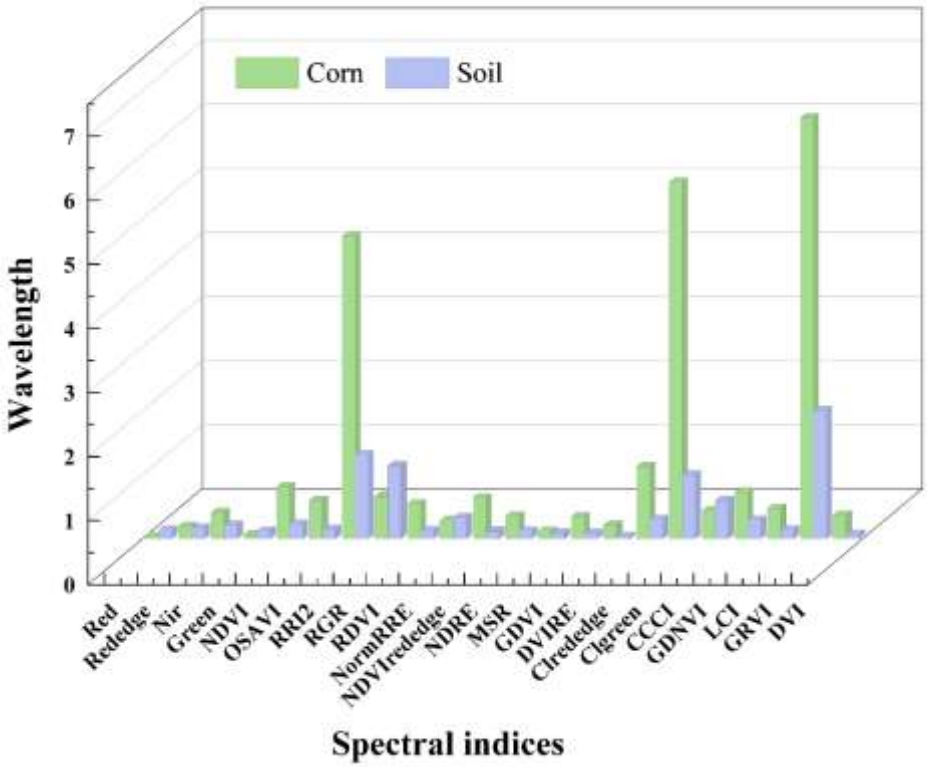

Figure 2. Difference of spectral reflectance between soil and corn.

3.2. Screening of Vis

This study, based on a feature-weight evaluation approach, uses random forests to perform sensitivity screening of VIs (Fig 3). From the 18 calculated VIs, the top 6 indices with variable importance values exceeding the 0.05 threshold were selected. These are: DVI (0.175548), CIrededge (0.143871), GNDVI (0.127267), NDRE (0.127179), CCCI (0.098620), and NDVIrededge (0.085003). They are all related to the red edge (RE) and near-infrared (NIR) bands, and can effectively capture changes in vegetation parameters such as chlorophyll content, leaf area index, and canopy cover. When corn is infested by leaf mites, small yellowish-white spots appear on the leaves, leading to a decrease in the plant's chlorophyll content and leaf coverage. Therefore, utilizing these sensitive VIs offers significant advantages in distinguishing healthy from damaged corn plants, providing reliable spectral features for subsequent pest monitoring.

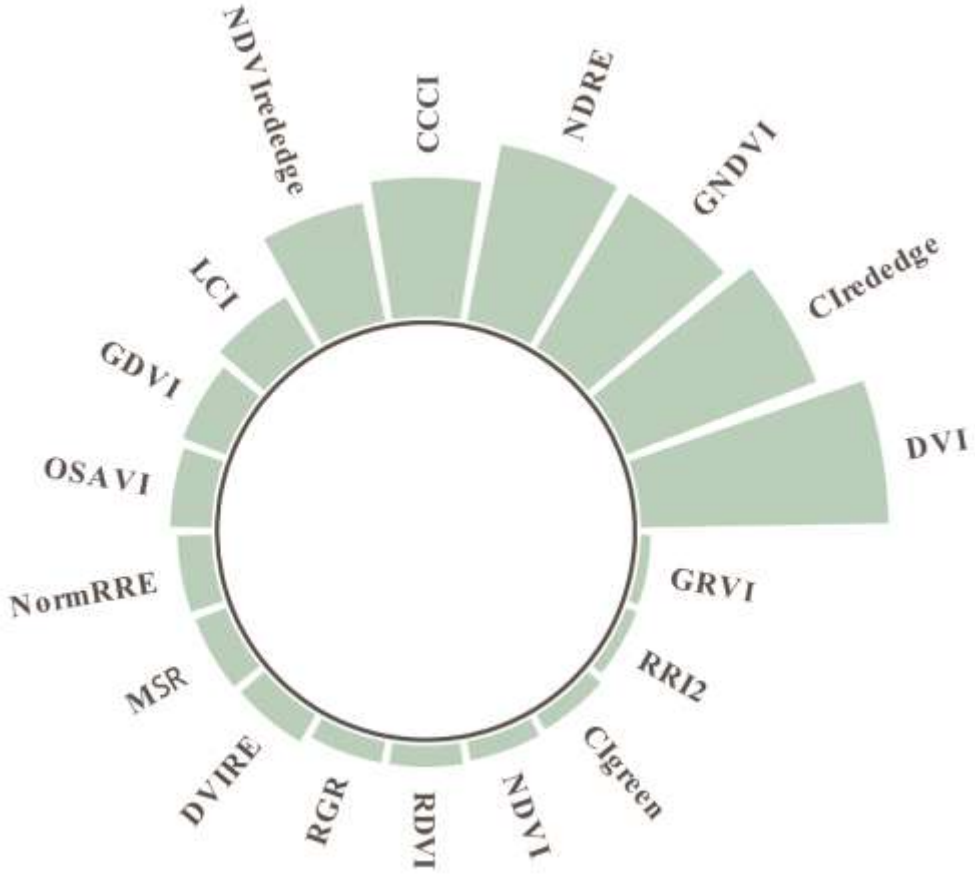

Figure 2. Difference of spectral reflectance between soil and corn.

3.3. Screening of Tis

When plants are attacked by leaf mites, both their morphological structure and spectral information undergo changes, leading to the manifestation of corresponding symptoms [13]. Using four spectral bands from multispectral imagery, four types of texture features were extracted, yielding 16 different TFs in total, and three TIs—NDTI, DTI, and RTI—were constructed, each consisting of two parts, T1 and T2. Each TIs contains 240 different combinations, for a total of 720 images of different combinations. A random forest algorithm was employed to analyze the 240 images corresponding to each spectral index in order to determine the most effective combination for CLM monitoring. Given the vast number of possible combinations, this research emphasizes showcasing the top 15 combinations with the highest weights for each texture index from the 240 available possibilities. Figures 5a-c illustrate the weights of these leading 15 combinations for NDTI, RTI, and DTI, respectively. Following the screening process, the superior combination of the three texture indices is presented in Table 5.

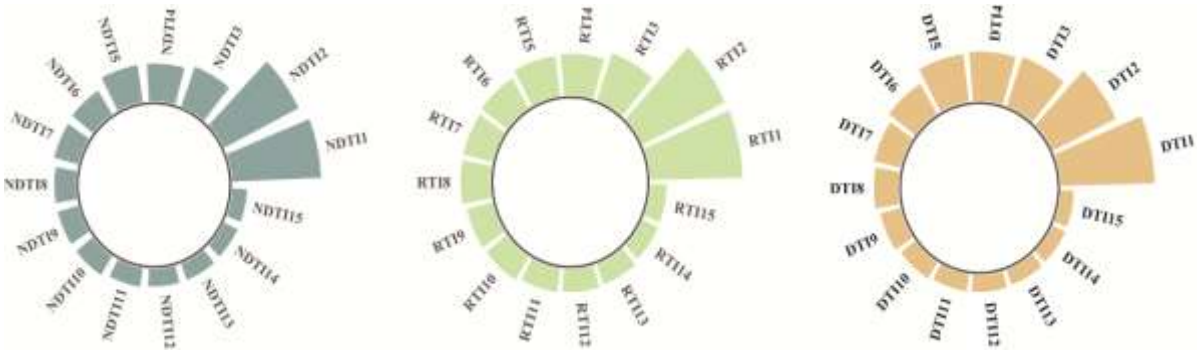

Figure 4. Importance distribution of the top 15 combinations with the highest texture index weights

Table 5 The best combination of texture index

Texture Index	T1	T2	Weight
NDTI	$Mean_{nir}$	$Mean_{rededge}$	0.0814
RTI	$Mean_{nir}$	$Mean_{rededge}$	0.0779
DTI	$Mean_{rededge}$	$Mean_{nir}$	0.0782

3.4. Model Performance Comparison and Analysis

To validate the applicability of different classification models under varying feature combinations, this study evaluated six monitoring models constructed using three algorithms (BPNN, PSO-SVM, and XGBoost) (Table 6). Select the top six VIs with the highest weights (DVI, CIrededge, GNDVI, NDRE, CCCI, and NDVIrededge) as input features, and simultaneously construct NDTI, DTI, and RTI as input features for the TIs.

Table 6. Accuracy evaluation table for six models

Features	Models	Parameters	Test set			
			Accuracy %	Precision %	Recall%	F1%
	BPNN	hidden layer sizes=50	91.33	91.00	92.39	92.14
Vis	PSO-SVM	gamma =1.04, c = 0.240	91.33	90.68	91.33	91.21
	XGBoost	n_estimators=50, threshold =0.5	89.40	89.43	90.38	89.67
	BPNN	Hidden layer sizes= (150, 100)	93.47	93.14	94.27	93.64
Vis+Tls	PSO-SVM XGBoost	gamma =64.45, c =0.097 n_estimators=100, threshold=0.5	93.27 91.32	92.44 91.00	93.00 92.13	93.04 91.21

In this experiment, vegetation indices and their combinations with texture indices were used as input features, and the effects of different feature inputs on the performance of three models were systematically investigated (Fig. 5), aiming to more effectively capture spatial structural information related to early CLM damage. From the figure, it can be seen that when VIs and TIs are used together as feature inputs, the model's accuracy, precision, recall, and F1 score are all better than the evaluation results using VIs alone.

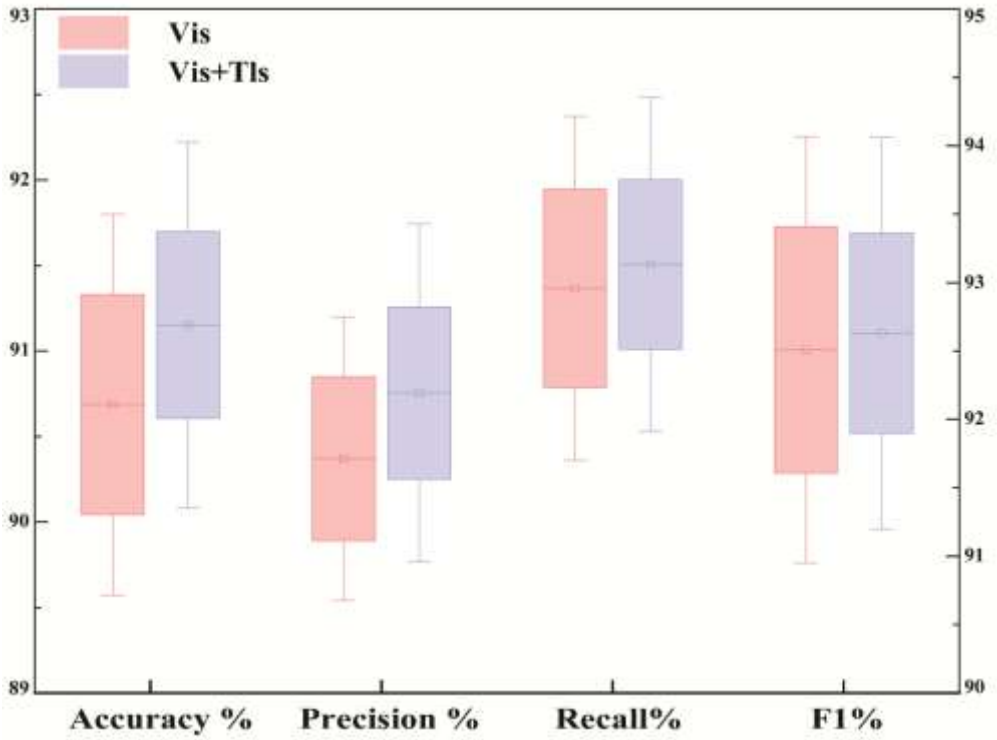

Figure 5. Differences in model evaluation indexes between different inputs

The recognition performance of BPNN, PSO-SVM, and XGBoost models was simultaneously compared (Fig 6). The figure shows the differences in accuracy of these models in pest monitoring. As can be seen from the figure, under different feature combinations the BPNN model performs best overall, followed by the PSO-SVM and XGBoost models. The BPNN model achieved an accuracy of 93.47% and an F1 score of 93.64%, meeting the accuracy requirements for early harm monitoring of CLM.

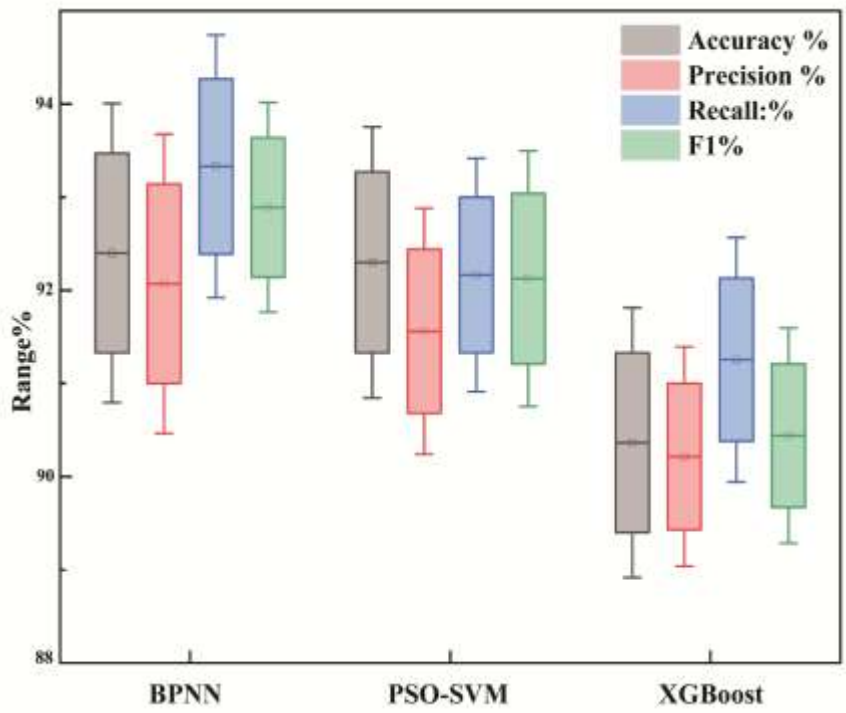

Figure 6. Comparison of evaluation indexes of different models.

In order to verify the superiority of TIs, the effects of TFs and TIs were compared in CLM monitoring. Use a random forest to screen 16 TFs and select the three with the highest weights as input features. In the BPNN model, VIs were respectively fused with TFs and TIs as input features for modeling (Fig. 7). As shown in the figure, the accuracy of the vegetation index combined with texture features (90.00%) is lower than that of the vegetation and texture indices (93.47%), and precision, recall, and F1 score show a similar trend. This clearly indicates that applying an exponential transform to the TFs can effectively enhance the subtle spatial structural information associated with early CLM damage, thereby achieving better performance than using the TFs directly and enabling the model to focus more on microscopic features specific to CLM damage—such as spatial lesions and leaf deformation—thus improving classification robustness and accuracy

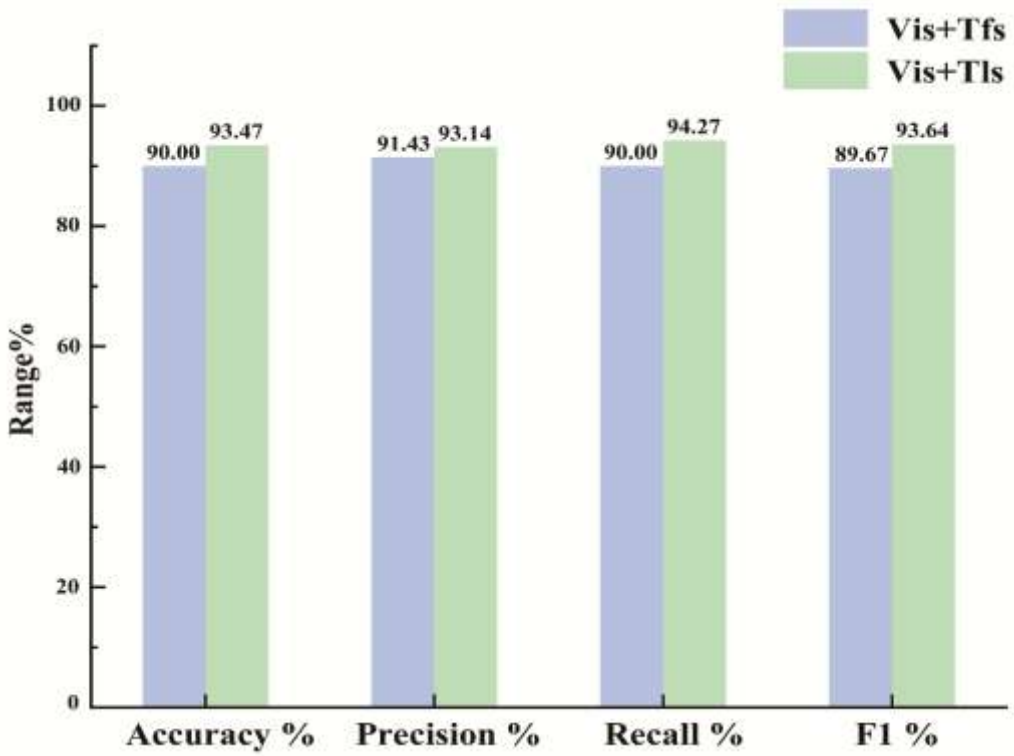

Figure 7. Comparison of the monitoring effects of TFs and TIs on corn spider mite.

3.5. Monitoring Results

Utilizing a BPNN model, TIs and VIs were combined as input features to conduct pixel-level classification monitoring of early CLM damage within the study area, ultimately resulting in the generation of a spatial distribution map for early CLM damage (Fig. 8). The figure clearly shows that overall corn damage in the study area during this period was relatively minor. Damage was more severe along field edges than in central areas, exhibiting a spatial pattern of scattered spots spreading outward—consistent with field observations.

Figure 8. Spatial distribution of corn spider mites.

4. Discussion

Using spectral and textural information derived from UAV remote sensing to efficiently and accurately monitor early CLM damage is essential for guiding the implementation of field management strategies in maize seed production and for achieving smart agriculture [9,64]. In earlier research, multispectral imagery has been utilized for tracking plant pest infestations. However, most early studies still mainly rely on spectral indices, such as NDVI and other vegetation indices [9,13], which often face accuracy bottlenecks when monitoring early-stage or asymptomatic pests and diseases, because these methods may struggle to adequately capture the subtle changes in crop morphology and texture caused by the occurrence and development of pests and diseases. Recently, as the capability to acquire high-resolution remote sensing data improves, scientists have endeavored to integrate TFs into the detection of plant pests to enhance monitoring precision [12,60,65]. In UAV remote sensing images, TFs represent the spatial arrangement of neighboring pixel brightness and distinct information, Provides monitoring information beyond spectral data for disease and pest monitoring, the combination of spectral and texture features allows for a more thorough understanding of the changes in plant pest development, ultimately contributing to improved monitoring accuracy [66]. On this basis, this study further explored the ability to monitor early CLM damage under field conditions by fusing spectral and texture information from UAV remote sensing with machine learning algorithms (BPNN, PSO-SVM, XGBoost). The results show that this method performs excellently in improving the early recognition accuracy of CLM; in particular, the BPNN model demonstrated the best monitoring performance among the three machine learning models (Fig. 6), achieving an accuracy of 93.47% and an F1 score of 93.64%. Provides reliable technical support for the rapid, non-destructive monitoring of early CLM damage under field conditions.

4.1. Effectiveness of spectral and texture feature selection

Remote sensing technology can reveal the physiological and biochemical changes in corn under CLM stress through spectral data [67,68]. However, CLM also causes point-like or patchy morphological damage to maize at spatial scales. This kind of small-scale spatial heterogeneity can be quantified by texture information, thereby supplementing the spatial-structural information from spectral monitoring and helping to improve the robustness of binary classification [12,60]. Therefore, this study proposes integrating spectral and textural indices to improve the accuracy of early CLM damage monitoring. The four original spectral bands derived from image data are insufficient to effectively distinguish corn from soil. Therefore, VIs are employed to enhance the contrast between corn plants and soil, thereby eliminating background interference. The study

found that using CIgreen can relatively clearly distinguish corn plants from soil (Fig. 2). Therefore, the Otsu-CIgreen algorithm is used to find the optimal threshold to distinguish soil from corn plants, thereby effectively removing the image background, this preprocessing has been shown to significantly improve subsequent classification accuracy, for example in monitoring southern blight in peanuts [26].

In terms of feature selection, First, use the random forest algorithm to select vegetation indices sensitive to CLM, retaining the top 6 by weight. At the same time, three texture indices (NDTI, RTI, DTI) were constructed based on 16 computed texture features. The optimal combination for each texture index was selected using the random forest algorithm. This process accomplishes effective dimensionality reduction of the original high-dimensional features, balancing information content and model robustness, and is consistent with recent practices in pest and disease remote sensing research that use data-driven feature selection to enhance model generalization [12,68]. Based on the above feature set, Using BPNN, PSO-SVM, and XGBoost algorithms, and taking VIs and the fusion of VIs and TIs as input features respectively, six models were established (Table 6). Among them, when modeling using only VIs, the BPNN model achieved a test accuracy of 91.33%, it demonstrated the feasibility of UAV multispectral imagery for early monitoring of CLM. When modeling by fusing VIs and TIs, the BPNN model's test accuracy reached 93.47%, demonstrate that incorporating TIs can bring significant gains on top of existing spectral information. In this study, the accuracy of modeling information using the fusion of VIs and TIs was higher than that using VIs alone. This may be because spectral features are more sensitive to changes in the leaf's internal physicochemical properties (such as chlorophyll content, changes in cell structure, etc.), while TIs reflect changes in the spatial distribution and structure of leaves and the canopy (for example, punctate necrosis, patchy distribution). The two are complementary, enabling the model to capture both intrinsic physiological changes and external morphological changes, thereby improving classification discriminative ability and, in turn, enhancing monitoring accuracy.

To further explore the advantages of incorporating TIs, this study used comparative experiments to demonstrate that TIs outperform TFs in extracting spatial structural information of early-stage hazards in CLM. Compared with modeling using only VIs or fusing VIs with TFs, when VIs were fused with TIs the BPNN model's test accuracy reached 93.47%, significantly higher than other schemes (Fig. 8). This indicates that applying an exponential transform to the TFs can more effectively extract canopy spatial structural information related to early CLM damage, thus outperforming the direct use of the original texture features. Spectral data are more sensitive to changes in the leaf's internal physicochemical properties (e.g., chlorophyll content, cellular structural changes), while texture reflects changes in the spatial distribution and structure of leaves and canopies (e.g., pinpoint necrosis, patchy distributions). They complement each other, allowing models to capture both intrinsic physiological changes and external morphological changes simultaneously, thereby improving classification performance. Overall, this study significantly improved the accuracy of early CLM monitoring under field conditions by combining spectral information with indexed and optimally combined texture information, and validated the effectiveness and application potential of TIs in early CLM recognition.

4.2. Limitations and Future Research

We acknowledge that this study has some limitations. First, our dataset is relatively small, which to some extent limits the model's ability to capture texture variations at different scales. To improve the model's generalization and robustness, and to fully validate the model's spatiotemporal reproducibility, it will be necessary in the future to build a larger-scale, cross-regional, multi-temporal multispectral pest sample database so as to systematically evaluate the model's replicability under different geographical and cultivation conditions (currently most related studies are conducted in a single experimental area) [9,11,13]. Secondly, this study mainly based its classification on single time-point data and did not fully utilize the temporal information in the pest development process. Multi-temporal data may provide richer features of pest evolution; combining time-series analysis or temporal deep learning models could further enhance early-warning capabilities. In addition, the current study uses only multispectral data; future research will consider integrating thermal infrared, hyperspectral, and other sensor data to supplement physiological and structural

information beyond spectral and textural features, thereby building a more comprehensive monitoring system. Despite these limitations, our study remains one of the first efforts to explore the potential advantages of multispectral imagery and machine learning algorithms for CLM monitoring under field conditions.

5. Conclusions

This study developed a method that combines spectral and texture indexing to improve the accuracy of early CLM damage monitoring. First extract 18 VIs related to CLM stress and construct 3 TIs. Then use Random Forest to select sensitive features and obtain the optimal feature set. On this basis, using VIs and the combination of VIs and TIs as input features, respectively, we constructed three types of monitoring models—BPNN, PSO-SVM, and XGBoost—and systematically compared their performance. The results show that the combined features based on the BPNN model performed best, with the test set accuracy reaching 93.47%, precision 93.14%, recall 94.27%, and an F1 score of 93.64%. In short, the integration of vegetation indices and texture indices derived from UAV multispectral data as features in machine learning significantly enhances the early damage identification capability of CLM. Excels at monitoring early damage from corn leaf mites, this provides reliable technical support for the rapid and non-destructive monitoring of CLM under field conditions and lays a practical foundation for the refined management of corn seed production.

Data Availability

The data and materials used and/or analyzed during the current study are available from the corresponding author on reasonable request.

Funding: Ministry of Agriculture and Rural Affairs' Scientific Research Base Project for Whole-Process Mechanization of Corn Seed Production (2105-000000-20-01-849645). Hexi College President's Fund Innovation Team Project (CXTD202404).

References

1. Xue, H.; Xu, X.P.; Meng, X. Estimation model for maize multi-components based on hyperspectral data. Sensors. 24,1-18. https://doi.org/10.3390/s24186111 (2024).
2. Bui, H.; Greenhalgh, R.; Gill, G.S.; Ji, M.; Kurlovs, A.H.; Ronnow, C, er al. Maize inbred line B96 is the source of large-effect loci for resistance to generalist but not specialist spider mites. Front. Plant Sci. 12,1-15. https://doi.org/10.3389/fpls.2021.693088 (2021).
3. Martin, D.E.; Latheef, M.A. Aerial application methods control spider mites on corn in Kansas, USA. Exp. Appl. Acarol. 77,571-582. https://doi.org/10.1007/s10493-019-00367-3 (2019).
4. Ruckert, A.; Golec, J.R.; Barnes, C.L.; Ramirez, R.A. Banks grass mite (Acari: Tetranychidae) suppression may add to the benefit of drought-tolerant corn hybrids exposed to water stress. J. Econ. Entomol. 114,187-196. https://doi.org/10.1093/jee/toaa269 (2021).
5. Rocandio-Rodríguez, M.; Torres-Castillo, J.A.; Juárez-Aragón, M.C.; Chacón-Hernández, J.C.; Moreno-Ramírez, Y.d.R.; Mora-Ravelo, S.G, er al. Evaluation of resistance of eleven maize races (Zea mays L.) to the red spider mite (Tetranychus merganser, Boudreaux). Plants. 11,1-22. https://doi.org/10.3390/plants11114144 (2022).
6. Zhang, J.C.; Huang, Y.B; Pu, R.L.; Gonzalez-Moreno, P.; Yuan, L.; Wu, K.H, er al. Monitoring plant diseases and pests through remote sensing technology: A review. Comput. Electron. Agr. 165,1-14. https://doi.org/10.1016/j.compag.2019.104943 (2019).
7. Abd El-Ghany, N.M.; Abd El-Aziz, S.E.; Marei, S.S. A review: application of remote sensing as a promising strategy for insect pests and diseases management. Environ. Sci. Pollut. R. 27,33503-33515. https://doi.org/10.1007/s11356-020-09517-2 (2020).
8. Wu, Y.; Li, X.C.; Zhang, Q.; Zhou, X.Z.; Qiu, H.B.; Wang, P.P. Recognition of spider mite infestations in jujube trees based on spectral-spatial clustering of hyperspectral images from UAVs. Front. plant Sci. 14, 1-19. https://doi.org/10.3389/fpls.2023.1078676 (2023).
9. Zhao, R.X.; Zhang, B.Y.; Zhang, C.M.; Chen, Z.Y.; Chang, N.; Zhou, B.Y, er al. Goji disease

and pest monitoring model based on unmanned aerial vehicle hyperspectral images. Sensors. 24,1-15. https://doi.org/10.3390/s24206739 (2024).

10. Tao, W.C.; Wang, X.S.; Xue, J.H.; Su, W.; Zhang, M.Z.; Yin, D.Q, er al. Monitoring the damage of armyworm as a pest in summer corn by unmanned aerial vehicle imaging. Pest Manag. Sci. 78,2265-2276. https://doi.org/10.1002/ps.6852 (2022).
11. Lv, Z.G.; Xu, B.Y.; Zhong, L.H.; Chen, G.S.; Huang, Z.H.; Sun, R, er al. Improved monitoring of southern corn rust using UAV-based multi-view imagery and an attention-based deep learning method. Comput. Electron. Agr. 224,1-12. https://doi.org/10.1016/j.compag.2024.109232 (2024).
12. Zou, M.X.; Liu, Y.; Fu, M.D.; Li, C.J.; Zhou, Z.X.; Meng, H.R, er al. Combining spectral and texture feature of UAV image with plant height to improve LAI estimation of winter wheat at jointing stage. Front. plant Sci. 14,1-19 https://doi.org/10.3389/fpls.2023.1272049 (2024).
13. Guo, W.; Gong, Z.; Gao, C.F.; Yue, J.B.; Fu, Y.Y.; Sun, H.G, er al. An accurate monitoring method of peanut southern blight using unmanned aerial vehicle remote sensing. Precis. Agric. 25,1857-1876 https://doi.org/10.1007/s11119-024-10137-w (2024).
14. Fan, Y.Y.; Wang, T.; Qiu, Z.J.; Peng, J.Y.; Zhang, C.; He, Y. Fast detection of striped stem-borer (Chilo suppressalis Walker) infested rice seedling based on visible/near-infrared hyperspectral imaging system. Sensors. 17, 1-13. https://doi.org/10.3390/s17112470 (2017).
15. Liu, X.D.; Wang, J.H. Developing spectral indices and models for monitoring rice planthoppers (Hemiptera: Delphacidae) with hyperspectral data and machine learning. J. Econ. Entomol. 118,2290-2300. https://doi.org/10.1093/jee/toaf214 (2025).
16. He, A.Q.; Xu, Z.H.; Li, G.T; Chen, L.Y.; Zhang, H.F.; Li, B, er al. Accurate estimation of aboveground biomass in Moso bamboo (Phyllostachys edulis) forests under Pantana phyllostachysae Chao stress using UAV multispectral remote sensing and self-establish allometric equations. Pest Manag. Sci. 81, 6650-6666. https://doi.org/10.1002/ps.70018 (2025)
17. Meng, R.; Gao, R.J.; Zhao, F.; Huang, C.Q.; Sun, R.; Lv, Z.G, er al. Landsat-based monitoring of southern pine beetle infestation severity and severity change in a temperate mixed forest. Remote sens. environ. 269, 1-17. https://doi.org/10.1016/j.rse.2021.112847(2022)
18. Tian, L.; Xue, B.W.; Wang, Z.Y.; Li, D.; Yao, X.; Cao, Q, er al. Spectroscopic detection of rice leaf blast infection from asymptomatic to mild stages with integrated machine learning and feature selection. Remote sens. environ. 257,1-16. https://doi.org/10.1016/j.rse.2021.112350 (2021)
19. Chithambarathanu, M.; Jeyakumar, M.K. Survey on crop pest detection using deep learning and machine learning approaches. Multimed. Tools Appl. 82, 42277-42310. https://doi.org/10.1007/s11042-023-15221-3(2023).
20. Kang, C.R.; Jiao, L.; Liu, K.; Liu, Z.G.; Wang, R.J. Precise crop pest detection based on co-ordinate-attention-based feature pyramid module. Insects 16,1-17. https://doi.org/10.3390/insects 16010103 (2025).
21. Barthlott, W.; Mail, M.; Bhushan, B.; Koch, K. Plant surfaces: structures and functions for biomimetic innovations. Nano-Micro Lett. 9, 1-40. https://doi.org/ 10.1007/s40820-016-0125-1 (2017).
22. Zhao, B.H.; Kang, X.L.; Zhou, H.; Shi, Z.Y.; Li, L.; Zhou, G.X, er al. Sparse-MoE-SAM: a lightweight framework integrating MoE and SAM with a sparse attention mechanism for plant disease segmentation in resource-constrained environments. Plants. 14,1-39. https://doi.org/10.3390/plants14172634 (2025).
23. Shen, T.T.; Zhang, C.; Liu, F.; Wang, W.; Lu, Y.; Chen, R.Q, er al. High-throughput screening of free proline content in rice leaf under

cadmium stress using hyperspectral imaging with chemometrics. Sensors. 20, 1-14. https://doi.org/10.3390/s20113229 (2020).
24. Genuer, R.; Poggi, J.M.; Tuleau-Malot, C. Variable selection using random forests. Pattern recogn. lett. 31, 2225-2236. https://doi.org/10.1016/j.patrec.2010.03.014 (2010).
25. Schwenker, F. Ensemble methods: Foundations and algorithms. IEEE Comput. Intell. M. 8, 77-79. https://doi.org/10.1109/MCI.2012.2228600 (2013).
26. Guo, Y.M.; Wang, Y.; Meng, K.; Zhu, Z.N. Otsu multi-threshold image segmentation based on adaptive double-mutation differential evolution. Biomimetics. 8,1-22. https://doi.org/10.3390/biomimetics8050418 (2023).
27. Cao, J.F.; Cui, H.Y.; Shi, H.; Jiao, L.J. Big Data: A parallel particle swarm optimization-back-propagation neural network algorithm based on MapReduce. PLoS One. 11,1-17. https://doi.org/10.1371/journal.pone.0157551 (2016).
28. Zou, G.Y.; Xiao, Y.Z.; Wang, M.S.; Zhang, H.M. Detection of bitterness and astringency of green tea with different taste by electronic nose and tongue. PLoS One. 13,1-10. https://doi.org/10.1371/journal.pone.0206517 (2018).
29. Du, X.X.; Liu, M.Y.; Sun, Y.H. Cell recognition using BP neural network edge computing. Contrast Media Mol. I. 2022, 1-7. https://doi.org/10.1155/2022/7355233 (2022).
30. Wang, Y.; Meng, X.C.; Zhu, L.Q. Cell group recognition method based on adaptive mutation PSO-SVM. Cells. 7,1-11. https://doi.org/10.3390/cells7090135 (2018).
31. Alzoubi, S.; Jawarneh, M.; Bsoul, Q.; Keshta, I.; Soni, M.; Khan, M.A. An advanced approach for fig leaf disease detection and classification: Leveraging image processing and enhanced support vector machine methodology. Open Life Sci. 18, 1-11. https://doi.org/10.1515/biol-2022-0764 (2023).
32. Lian, Y.Y.; Wang, A.Q.; Peng, S.H.; Jia, J.J; Zong, L.; Yang, X.F, er al. Optimization of sensors data transmission paths for pest monitoring based on intelligent algorithms. Biosensors. 12,1-12. https://doi.org/10.3390/bios12110948 (2022).
33. Skendžić, S.; Zovko, M.; Živković, I.P.; Lešić, V.; Lemić, D. The impact of climate change on agricultural insect pests. Insects. 12, 1-31. https://doi.org/10.3390/insects12050440 (2021).
34. Wang, N.; Guo, Y.C.; Wei, X.; Zhou, M.T.; Wang, H.J.; Bai, Y.B. UAV-based remote sensing using visible and multispectral indices for the estimation of vegetation cover in an oasis of a desert. Ecol. Indic. 141, 1-14. https://doi.org/10.1016/j.ecolind.2022.109155 (2022).
35. Odilbekov, F.; Armoniené, R.; Henriksson, T.; Chawade, A. Proximal phenotyping and machine learning methods to identify Septoria tritici blotch disease symptoms in wheat. Front. plant sci. 9,1-11. https://doi.org/10.3389/fpls.2018.00685 (2018).
36. Yue, J.B.; Feng, H.K.; Jin, X.L; Yuan, H.H.; Li, Z.H.; Zhou, C.Q, er al. A comparison of crop parameters estimation using images from UAV-mounted snapshot hyperspectral sensor and high-definition digital camera. Remote Sensing 10, 1-24. https://doi.org/10.3390/rs10071138 (2018).
37. Mishra, S.; Mishra, D.R. Normalized difference chlorophyll index: A novel model for remote estimation of chlorophyll-a concentration in turbid productive waters. Remote Sens. Environ. 117,394-406. https://doi.org/10.1016/j.rse.2011.10.016 (2012).
38. Phadikar, S.; Sil, J.; Das, A.K. Vegetative indices and edge texture based shadow elimination method for rice plant images. In Proceedings of the 2012 International conference on radar, communication and computing (ICRCC), pp, 1-5. https://doi.org/10.1109/ICRCC.2012.6522596. (2012).
39. Zhou, J.; Yungbluth, D.; Vong, C.N.; Scaboo, A.; Zhou, J.F. Estimation of the maturity date of soybean breeding lines using UAV-based multispectral imagery. Remote Sensing. 11, 1-

17. https://doi.org/10.3390/rs11182075 (2019).
40. Patrick, A.; Pelham, S.; Culbreath, A.; Holbrook, C.C.; De Godoy, I.J.; Li, C.Y. High throughput phenotyping of tomato spot wilt disease in peanuts using unmanned aerial systems and multispectral imaging. IEEE Instru. Meas. Mag. 20, 4-12. https://doi.org/ 10.1109/ MIM.2017.7951684 (2017).
41. Gitelson, A.; Merzlyak, M.N. Quantitative estimation of chlorophyll-a using reflectance spectra: Experiments with autumn chestnut and maple leaves. J. Photoch. Photobio. B. 22, 247-252. https://doi.org/10.1016/1011-1344(93)069 63-4 (1994).
42. Gitelson, A.A.; Kaufman, Y.J.; Merzlyak, M.N. Use of a green channel in remote sensing of global vegetation from EOS-MODIS. Remote sens. Environ. 58, 289-298. https://doi.org/10. 1016/S0034-4257(96)00072-7 (1996).
43. Zheng, H.B.; Cheng, T.; Zhou, M.; Li, D.; Yao, X.; Tian, Y.C, er al. Improved estimation of rice aboveground biomass combining textural and spectral analysis of UAV imagery. Precis. Agric. 20,611-629. https://doi.org/10.1007/s1 1119-018-9600-7 (2019).
44. Chivasa, W.; Mutanga, O.; Burgueño, J. UAV-based high-throughput phenotyping to increase prediction and selection accuracy in maize varieties under artificial MSV inoculation. Comput. Electron. Agr. 184, 1-14. https://doi. org/10.1016/j.compag.2021.106128 (2021).
45. Kerkech, M.; Hafiane, A.; Canals, R. Deep leaning approach with colorimetric spaces and vegetation indices for vine diseases detection in UAV images. Comput. Electron. Agr. 155, 237-243. https://doi.org/10.1016/j.compag.2018.10. 006 (2018).
46. Irmak, S.; Haman, D.Z.; Bastug, R. Determination of crop water stress index for irrigation timing and yield estimation of corn. Agron. j. 92, 1221-1227. https://doi.org/10.2134 /agronj2000.9261221x (2000).
47. Rondeaux, G.; Steven, M.; Baret, F. Optimization of soil-adjusted vegetation indices. Remote sens. Environ. 55, 95-107. https://doi.org/10.1016/0034-4257(95)00186-7 (1996).
48. Huang, H.S; Deng, J.Z.; Lan, Y.B; Yang, A.Q.; Zhang, L.; Wen, S, er al. Detection of helminthosporium leaf blotch disease based on UAV imagery. Applied Sciences. 9, 1-12. https://doi.org/10.3390/app9030558 (2019).
49. Bai, L.G.; Huang, X.J.; Dashzebeg, G.; Ariunaa, M.; Yin, S.; Bao, Y.H, er al. Potential of unmanned aerial vehicle red–green–blue images for detecting needle pests: A case study with erannis jacobsoni djak (Lepidoptera, Geometridae). Insects. 15,172. https://doi.org /10.3390/insects15030172 (2024).
50. Ma, Y.R.; Ma, L.L.; Zhang, Q.; Huang, C.P.; Yi, X.; Chen, X.Y, er al. Cotton yield estimation based on vegetation indices and texture features derived from RGB image. Front. Plant Sci. 13, 1-17. https://doi.org/10.3 389/fpls.2022.925986 (2022).
51. Liu, Y.; Feng, H.K.; Yue, J.B.; Jin, X.L.; Li, Z.H.; Yang, G.J. Estimation of potato above-ground biomass based on unmanned aerial vehicle red-green-blue images with different texture features and crop height. Front. Plant Sci. 13,1-18. https://doi.org/10.3389/fpls.2022. 938216 (2022).
52. Tang, Z.J.; Lu, J.H.; Abdelghany, A.E.; Su, P.H.; Jin, M.; Li, S.Q, er al. Winter oilseed rape LAI inversion via multi-source UAV fusion: A three-dimensional texture and machine learning approach. Plants. 14, 1-19. https://doi.org/10. 3390/plants14081245 (2025).
53. Xie, C.Q.; He, Y. Spectrum and image texture features analysis for early blight disease detection on eggplant leaves. Sensors. 16, 1-15. https://doi.org/10.3390/s16050676 (2016).
54. Shi, H.Z.; Liu, Z.Y.; Li, S.Q.; Jin, M.; Tang, Z.J.; Sun, T, er al. Monitoring soybean soil moisture content based on UAV multispectral and thermal-infrared remote-sensing information fusion. Plants. 13, 1-20. https:// doi.org/10.3390/plants13172417 (2024).

55. Lu, H.; Liu, C.; Li, N.W.; Fu, X.; Li, L.G. Optimal segmentation scale selection and evaluation of cultivated land objects based on high-resolution remote sensing images with spectral and texture features. Environ. Sci. Pollut. R. 28, 27067-27083. https://doi.org/10.1007/s11356-021-12552-2 (2021).
56. Yao, Q.S.; Zhang, Z.; Lv, X.; Chen, X.Y.; Ma, L.L.; Sun, C. Estimation model of potassium content in cotton leaves based on wavelet decomposition spectra and image combination features. Front. Plant Sci. 13, 1-20. https://doi.org/10.3389/fpls.2022.920532 (2022).
57. Zhang, Y.H.; Liu, D.S. Rethinking feature representation and attention mechanisms in intelligent recognition of leaf pests and diseases in wheat. Sci. Rep-uk. 15, 1-12. https://doi.org/10.1038/s41598-025-99027-3 (2025).
58. Nyasulu, C.; Diattara, A.; Traore, A.; Ba, C.; Diedhiou, P.M.; Sy, Y, er al. A comparative study of machine learning-based classification of tomato fungal diseases: Application of GLCM texture features. Heliyon. 9. 1-12. https://doi.org/10.1016/j.heliyon.2023.e21697 (2023).
59. Yang, W.L.; Li, Z.J.; Chen, G.F.; Cui, S.H.; Wu, Y.; Liu, X.C, er al. Soybean (glycine max L.) leaf moisture estimation based on multisource unmanned aerial vehicle image feature fusion. Plants. 13, 1-14. https://doi.org/10.3390/plants13111498 (2019).
60. Sun, X.K.; Yang, Z.Y.; Su, P.Y.; Wei, K.X.; Wang, Z.G.; Yang, C.B, er al. Non-destructive monitoring of maize LAI by fusing UAV spectral and textural features. Front. Plant Sci. 14,1-11. https://doi.org/10.3389/fpls.2023.1158837 (2023).
61. Guo, H.R.; Cheng, Y.H.; Liu, J.; Wang, Z.H. Low-cost and precise traditional chinese medicinal tree pest and disease monitoring using UAV RGB image only. Sci. Rep-uk. 14, 1-23. https://doi.org/10.1038/s41598-024-76502-x (2024).
62. Zhang, X.L.; Bu, J.Y.; Zhou, X.X; Wang, X.C. Automatic pest identification system in the greenhouse based on deep learning and machine vision. Front. Plant Sci. 14, 1-13. https://doi.org/10.3389/fpls.2023.1255719 (2023).
63. Zhang, H.S.; Huang, L.S.; Huang, W.J.; Dong, Y.Y.; Weng, S.Z.; Zhao, J.L, er al. Detection of wheat Fusarium head blight using UAV-based spectral and image feature fusion. Front. Plant Sci. 13, 1-14. https://doi.org/10.3389/fpls.2022.1004427 (2022).
64. Liu, W.T.; Xie, Z.R.; Du, J.; Li, Y.H.; Long, Y.B.; Lan, Y.B, er al. Early detection of pine wilt disease based on UAV reconstructed hyperspectral image. Front. Plant Sci. 15, 1-14. https://doi.org/10.3389/fpls.2024.1453761 (2024).
65. Sabzi, S.; Abbaspour-Gilandeh, Y.; Arribas, J.I. An automatic visible-range video weed detection, segmentation and classification prototype in potato field. Heliyon. 6, 1-17. https://doi.org/10.1016/j.heliyon.2020.e03685 (2020)
66. Zhao, S.Y.; Liu, J.Z.; Bai, Z.C.; Hu, C.H.; Jin, Y.J. Crop pest recognition in real agricultural environment using convolutional neural networks by a parallel attention mechanism. Front. Plant Sci.13, 1-14. https://doi.org/10.1038/s41598-024-76502-x (2022).
67. Xu, D.; Lu, Y.W.; Liang, H.; Lu, Z.; Yu, L.J.; Liu, Q. Areca yellow leaf disease severity monitoring using UAV-based multispectral and thermal infrared imagery. Remote Sensing. 15, 1-19. https://doi.org/10.3390/rs15123114 (2023).
68. Nguyen, C.; Sagan, V.; Skobalski, J.; Severo, J.I. Early detection of wheat yellow rust disease and its impact on terminal yield with multi-spectral UAV-imagery. Remote Sensing. 15,1-28. https://doi.org/10.3390/rs15133301 (2023).